Available online at www.sciencedirect.com
ScienceDirect
Journal of Solid State Chemistry 180 (2007) 3351–3359
JOURNAL OF SOLID STATE CHEMISTRY
www.elsevier.com/locate/jssc

Phase relations in the system K_2MoO_4–KPO_3–MoO_3–Bi_2O_3: A new phosphate $K_3Bi_5(PO_4)_6$

Kateryna V. Terebilenko[a], Igor V. Zatovsky[a,*], Nikolay S. Slobodyanik[a], Konstantin V. Domasevitch[a], Denis V. Pushkin[b], Vyacheslav N. Baumer[c], Valentina S. Sudavtsova[d]

[a]*Inorganic Chemistry Department, Kiev University, Volodimirska Street 64, Kiev 01033, Ukraine*
[b]*Samara State University, Ac. Pavlov St. 1, Samara 443011, Russian Federation*
[c]*STC "Institute for Single Crystals" NAS of Ukraine, 60 Lenin ave., Kharkiv 61001, Ukraine*
[d]*Physical Chemistry Department, Kiev University, Volodimirska Street 64, Kiev 01033, Ukraine*

Received 5 July 2007; received in revised form 1 October 2007; accepted 2 October 2007
Available online 4 October 2007

Abstract

Phase equilibrium in the pseudo-quaternary system K_2O–MoO_3–P_2O_5–Bi_2O_3 was studied as three-component solvent K_2MoO_4–KPO_3–MoO_3 containing 15 mol% Bi_2O_3 during slow cooling and spontaneous crystallization. The results of the investigation were shown on a composition diagram, which indicates the crystallization fields of $K_2Bi(PO_4)(MoO_4)$, $K_5Bi(MoO_4)_4$, $BiPO_4$ and $K_3Bi_5(PO_4)_6$. New phosphate $K_3Bi_5(PO_4)_6$ was characterized by single-crystal X-ray diffraction (space group $C2/c$, $a = 17.680(4)$, $b = 6.9370(14)$, $c = 18.700(4)$ Å, $\beta = 113.79(3)^\circ$) and FTIR spectroscopy. The possibility of lone electron pair stereoactivity of bismuth was suggested using the calculations of characteristics of the Voronoi–Dirichlet polyhedra for $K_3Bi_5(PO_4)_6$ and $K_2Bi(PO_4)(MoO_4)$.

Keywords: Composition diagram; Phosphate; Bismuth; Flux

1. Introduction

Bismuth phosphates and molybdates exhibit a wide range of properties, which make them useful materials for many modern technologies. For instance, $Ba_3Bi(PO_4)_3$ [1] and $Na_3Bi_5(PO_4)_6$ [2] with eulytite structure have possible applications in optical and optoelectronic domains (scintillators and lasers) [2], $Bi_{46}P_8O_{89}$ is a good ionic conductor [3]. Moreover, bismuth phosphates are reported to be excellent catalysts in different reactions. For example, $BiPO_4$, pure or doped with molybdenum, catalyzes the synthesis of butyraldehyde from 1-butanol [4]. Furthermore, bismuth molybdates are well-known catalysts for the various reactions of oxidative dehydrogenation [5–7]. Several recent works deal with the investigations of the spectroscopic and luminescent properties of complex bismuth molybdates with general compositions $M^IBi(MoO_4)_2$ [8] and $M^I_5Bi(MoO_4)_4$ [9] (M^I—alkaline metal). It was shown that single crystals of these molybdates possess the scintillating capability and nonlinear optical properties [8,10,11].

The significant interest in bismuth compounds for optical, optoelectronic and laser studies stimulates developing and improving of single-crystal growth methods. A number of investigations of binary Bi_2O_3–P_2O_5 and ternary M^I_2O–Bi_2O_3–P_2O_5 systems showed the existence of $Bi_{6.67}O_4(PO_4)_4$ [12], $K_2Bi_3O(PO_4)_3$ [13], $Na_3Bi(PO_4)_2$ [14] and $M^I_{0.5}Bi_{6.5}O_4(PO_4)_4$ (M^I—Li, Na, K) [15] phosphates. It should be stressed that these compounds were usually obtained using the solid-state technique. Using of the self-flux method leads to several difficulties, partially because of high viscosity and the tendency to glass formation in bismuth-containing phosphate systems [16,17]. As it was determined earlier, using the phosphate-molybdate or tungstate fluxes with their rather low viscosity and fine

*Corresponding author.
E-mail address: Zvigo@yandex.ru (I.V. Zatovsky).

0022-4596/$ - see front matter © 2007 Elsevier Inc. All rights reserved.
doi:10.1016/j.jssc.2007.10.001

solvent possibilities open an additional opportunity for successful crystal growth [18–21].

Our previous investigations in K_2MoO_4–MoO_3–KPO_3–Bi_2O_3 flux system have shown that this system creates favorable conditions for spontaneous crystallization of a new $K_2Bi(PO_4)(MoO_4)$ phosphate-molybdate [22]. It is reasonable to expect that more detailed investigation in this complex solution may characterize the stability region of this compound and reveal the possibility of the formation of new compounds.

2. Experimental

2.1. Phase equilibrium studies

The crystallization fields of various phases in the system were determined on the basis of the results obtained during slow cooling and spontaneous crystallization of numerous high-temperature solutions with various compositions. The system was considered as a K_2MoO_4–KPO_3–MoO_3 three-component solvent containing 15 mol%. Bi_2O_3. From this point of view, points on ternary diagram xK_2MoO_4–$yKPO_3$–$zMoO_3$ correspond to compositions of the quaternary system $0.85xK_2MoO_4$–$0.85yKPO_3$–$0.85zMoO_3$–$0.15Bi_2O_3$.

In a typical reaction, analytical reagent grade purity KPO_3, K_2MoO_4, MoO_3 and Bi_2O_3 in calculated molar rations were used for the preparation of the melts. The samples were heated up to 950–850 °C in a platinum crucible, and then kept at this temperature under stirring using a Pt stirrer until it became homogeneous. The high-temperature solutions were cooled down to 550–470 °C at a rate of 30–10° per hour and kept at those temperatures for 1–2 h depending on the melt composition, allowing spontaneous nucleation. Intensive stirring at final stages relieves the crystallization of over-cooled melts in several cases. At the end of crystallization the remaining flux was poured out on a sheet copper. Obtained products were leached out with boiling water. The phases were identified by optical microscopy and X-ray powder diffraction.

2.2. Preparation of $K_3Bi_5(PO_4)_6$

A new double phosphate with a general formula $K_3Bi_5(PO_4)_6$ for the structural investigations was prepared in the following way. A carefully ground mixture of 6.274 g K_2MoO_4, 4.076 g MoO_3, 15.835 g KPO_3 and 3.188 g Bi_2O_3 was placed in a platinum crucible and filled to 80% of its capacity with charge. The mixture corresponds to the nominal composition $13.7K_2O \cdot 8MoO_3 \cdot 9.8P_2O_5 \cdot Bi_2O_3$. The annealing time was 30 min at 850 °C and the cooling rate was equal to 10 °C/h from 720 to 470 °C under stirring. Colorless prismatic crystals, the linear dimensions of which typically exceed 0.2 mm, were obtained using the above-mentioned technique in 40% yield (by Bi).

The ICP determination of the potassium, phosphorus and bismuth amounts in prepared crystals was performed on a "Spectroflame Modula ICP" ("Sectro", Germany) instrument. Analysis shows that the K/Bi/P ratio is 3:5:6 for $K_3Bi_5(PO_4)_6$.

2.3. X-ray data collection and structure refinement

A colorless prismatic crystal of $K_3Bi_5(PO_4)_6$ with linear dimensions of $0.06 \times 0.05 \times 0.03\,mm^3$ was selected for single-crystal X-ray investigation. Diffraction data were collected on a STOE IPDS-I diffractometer at 210 K using a monochromatized Mo$K\alpha$ radiation ($\lambda = 0.71073$ Å). Table 1 lists the cell parameters and details of the data acquisition and structure refinement.

The structure was solved using the heavy atom method and refined in the full-matrix least-squares technique in the anisotropic approximation using the SHELXS-97 [23] and SHELXL-97 [24] program packages. Since it was impossible to calculate anisotropic displacement parameters for potassium atoms (non-positive definite), they were refined

Table 1
Crystallographic data and structure refinement parameters for $K_3Bi_5(PO_4)_6$

Crystal data	
Formula unit	$K_3Bi_5(PO_4)_6$
Formula weight	1732.02
Crystal system	Monoclinic
Space group	$C2/c$ (no. 15)
Cell parameters	
a (Å)	17.680(4)
b (Å)	6.9370(14)
c (Å)	18.700(4)
β (deg)	113.79(3)
V (Å^3)	2098.6(7)
Z	4
ρ_{cal} (g cm^{-1})	5.482
Intensity measurements	
Crystal dimensions (mm^3)	$0.06 \times 0.05 \times 0.03$
Measurement temperature (K)	210(2)
Apparatus	STOE IPDS
Wavelength (Å)	(Mo$K\alpha$) = 0.71073
Monochromator	Graphite
μ (mm^{-3})	42.960
Theta range	2.68–28.03°
Unique reflections, R_{eq}	6379, 0.0796
Retained reflections ($I > 2\sigma I$)	2443
h_{range}	$-23 \rightarrow 22$
k_{range}	$-9 \rightarrow 9$
l_{range}	$-22 \rightarrow 24$
F (000)	3016
Structure solution and refinement	
Absorption correction;	Multi-scan
T_{min}, T_{max}	0.0759, 0.2589
Resolution method	Heavy atom method
Agreement factors	$R_1 = 0.0647$; w$R = 0.1553$; $S = 1.072$
Number parameters	167
$(\Delta\rho)_{max,\ min}$ (e/Å^{-3})	3.273, −3.025
Weighting scheme	$W = 1/[\sigma^2(F_o^2) + (0.1370P)^2 + 111.4735P]$, where $P = (F_o^2 + 2F_c^2)/3$

Table 2
The coordinates and equivalent isotropic thermal parameters of the atoms for $K_3Bi_5(PO_4)_6$

Atom	Site	x	y	z	U_{eq}/U^*_{iso} (Å^2)
Bi1	8*f*	0.13621(4)	0.10275(9)	0.47262(4)	0.0212(3)
Bi2	8*f*	0.27559(4)	−0.10412(9)	0.70322(4)	0.0211(3)
Bi3	4*e*	1/2	−0.35935(17)	3/4	0.0269(3)
K1	8*f*	0.0770(2)	−0.3975(4)	0.5682(2)	0.0128(6)*
K2	4*e*	1/2	0.189(3)	3/4	0.106(5)*
P1	8*f*	0.3711(3)	−0.0859(6)	0.5911(3)	0.0216(9)
P2	8*f*	0.2818(3)	0.4044(5)	0.6490(3)	0.0160(8)
P3	8*f*	0.0719(3)	0.0831(6)	0.6162(2)	0.0157(9)
O1	8*f*	0.4227(9)	−0.1238(18)	0.6813(8)	0.026(3)
O2	8*f*	0.2811(9)	−0.067(2)	0.5848(8)	0.027(3)
O3	8*f*	0.4077(10)	0.1066(18)	0.5757(8)	0.025(3)
O4	8*f*	0.3819(11)	−0.248(2)	0.5412(9)	0.039(4)
O5	8*f*	0.2367(11)	0.339(2)	0.565(1)	0.039(4)
O6	8*f*	0.2853(10)	0.2411(17)	0.7067(7)	0.028(3)
O7	8*f*	0.2389(11)	0.571(2)	0.6707(9)	0.036(3)
O8	8*f*	0.3692(8)	0.456(2)	0.6565(8)	0.030(3)
O9	8*f*	0.1460(9)	−0.054(2)	0.6272(9)	0.030(3)
O10	8*f*	0.0928(9)	0.214(2)	0.6887(7)	0.027(3)
O11	8*f*	0.0553(8)	0.196(2)	0.5422(7)	0.026(3)
O12	8*f*	0.0006(8)	−0.049(2)	0.6149(7)	0.025(3)

isotropically. The coordinates and U_{eq}/U_{iso} of the atoms are listed in Table 2. These collected data and refining are better than other experiments for $K_3Bi_5(PO_4)_6$ crystals. Selected bond lengths and bond angles for this compound are shown in Table 3.

Further details of the crystal structure of $K_3Bi_5(PO_4)_6$ investigation are available from the Fachionformations-zentrum Karlsruhe, D-76344 Eggeinstein-Leopoldshafen (Germany), on quoting depository number CSD-418253.

The purity of the crystalline products and phase composition of the obtained mixtures were controlled and identified using powder X-ray diffraction. X-ray powder patterns were recorded at room temperature on DRON-2 and DRON-3 diffractometers with Cu$K\alpha$ radiation ($\lambda = 1.5418$ Å). Reference patterns from a database PDF2 were used to identify known crystal structures of $BiPO_4$ (HT) (PDF2 No. 43-0637) [25] and $K_5Bi(MoO_4)_4$ (PDF2 No. 29-0986) [26]. Powder X-ray diffraction data for $K_2Bi(PO_4)(MoO_4)$ were reported in our previous work [22].

2.4. Thermal analysis and FTIR spectroscopy

Differential thermal analysis (DTA) was carried out on a Quasy-1500 thermal analyser in the temperature range 20–1000 °C (heating rate 5 °C/min). The experiments were performed for a ground powder of selected single crystals of $K_2Bi(PO_4)(MoO_4)$ and $K_3Bi_5(PO_4)_6$, respectively.

The FTIR spectra were studied in the spectral range 400–1500 cm^{-1} and were collected at a room temperature in KBr discs using a NICOLET Nexus 470 (FTIR) spectrometer.

3. Results and discussion

3.1. Phase formation in the K_2MoO_4–KPO_3–MoO_3–Bi_2O_3 system

The experimental results of the system investigations allowed the construction of the proposed composition diagram (Fig. 1). It should be pointed out that this plot is not intended to give the exact phase boundaries but rather to show the approximate fields of phase formation. This approach, however, does give enough quantitative information to grow crystals of compounds that are presented here and shows several interesting trends in the molten system.

Generally, the composition diagram indicates the homogeneity regions for four pure compounds and two crystallization fields of phase coexistence. The largest homogeneity area was observed for the $K_2Bi(PO_4)(MoO_4)$, which grows in the MoO_3-deficit region with the K_2MoO_4/MoO_3 molar ratio equal to 5.40–4.25. Increasing of this ratio up to 6.45 leads to $K_5Bi(MoO_4)_4$ formation.

These two fields can be characterized as inserted ones in the K_2MoO_4–KPO_3–$K_2Mo_2O_7$ section. The cross-section KPO_3–$K_2Mo_2O_7$ divides the composition diagram into two sections. From this point of view, the second section KPO_3–$K_2Mo_2O_7$–MoO_3 should be described as an area of phosphates formation. Thus, a new double compound $K_3Bi_5(PO_4)_6$ crystallizes in case of molar ratio $K_2MoO_4/MoO_3 = 1.60$–0.85 and $KPO_3/K_2MoO_4 = 5.72$–1.85. Decreasing of the latter ratio to 1.28–1.00 causes formation of $K_3Bi_5(PO_4)_6$ and $K_2Bi(PO_4)(MoO_4)$ together.

It should be noted that without stirring during the crystallization process the crystals do not originate in several fields of the diagram describing the K_2MoO_4–KPO_3–MoO_3–Bi_2O_3 molten system, especially for the region of $K_3Bi_5(PO_4)_6$ formation. This phenomenon has been pointed out for crystallization of $K_2Bi(PO_4)(MoO_4)$, but in this case it is less pronounced. As a result, the stirring was effective in enhancing the crystallization process. We assume that gradual nucleation occurs on the platinum surfaces during the stirring of the melt.

The crystallization of $K_2Bi(PO_4)(MoO_4)$ had been detected at a temperature near 700 °C, while that of $K_3Bi_5(PO_4)_6$ was detected only near 550 °C. Whereas the DTA data indicate that the first compound melts at 710 °C, the second remains stable up to 1000 °C without melting.

Crystallization of bismuth orthophosphate $BiPO_4$ (high temperature form-HT) is observed in a wide range of molar ratios at high KPO_3 content, including the large fields of pure phase formation and the region with some additional content of double phosphate $K_3Bi_5(PO_4)_6$. Experimental points with $KPO_3/K_2MoO_4 = 4.18$–1.73 and $K_2MoO_4/MoO_3 = 0.46$–0.10 correspond to the cocrystallization of $BiPO_4$ (HT) and $K_3Bi_5(PO_4)_6$. This wide crystallization field cuts the region of the pure $BiPO_4$ (HT) formation into

Table 3
The bond lengths (Å) and bond angles (deg) in the coordination polyhedra for $K_3Bi_5(PO_4)_6$

BiO_8 polyhedra							
Bi(1)–O(3)^{i}	2.218(12)	O(3)^{vi}–Bi(1)–O(5)	73.8(6)	O(4)^{viii}–Bi(1)–O(8)^{vi}	77.0(5)	O(5)–Bi(1)–O(12)^{vii}	145.8(6)
Bi(1)–O(12)^{ii}	2.340(13)	O(3)^{vi}–Bi(1)–O(12)^{vii}	76.6(5)	O(4)^{viii}–Bi(1)–O(5)^{vi}	102.2(5)	O(5)^{vi}–Bi(1)–O(8)^{vi}	56.9(5)
Bi(1)–O(11)	2.379(13)	O(3)^{vi}–Bi(1)–O(11)	77.7(5)	O(4)^{viii}–Bi(1)–O(11)	104.2(5)	O(5)^{vi}–Bi(1)–O(12)^{vii}	126.0(5)
Bi(1)–O(8)^{i}	2.412(12)	O(3)^{vi}–Bi(1)–O(8)^{vi}	83.2(5)	O(4)^{viii}–Bi(1)–O(5)	138.0(6)	O(5)^{vi}–Bi(1)–O(11)	150.2(5)
Bi(1)–O(4)^{iii}	2.480(17)	O(3)^{vi}–Bi(1)–O(5)^{vi}	87.1(6)	O(5)–Bi(1)–O(5)^{vi}	69.1(5)	O(8)^{vi}–Bi(1)–O(12)^{vii}	70.1(4)
Bi(1)–O(5)	2.521(16)	O(3)^{vi}–Bi(1)–O(4)^{viii}	148.2(5)	O(5)–Bi(1)–O(11)	82.0(5)	O(8)^{vi}–Bi(1)–O(11)	143.5(5)
Bi(1)–O(5)^{i}	2.642(15)	O(4)^{viii}–Bi(1)–O(12)^{vii}	73.4(5)	O(5)–Bi(1)–O(8)^{vi}	121.9(4)	O(11)–Bi(1)–O(12)^{vii}	75.3(4)
Bi(1)–O(2)	2.831(24)						
Bi(2)–O(9)	2.183(15)	O(2)–Bi(2)–O(9)	78.0(5)	O(6)–Bi(2)–O(9)	84.4(5)	O(6)^{i}–Bi(2)–O(9)	83.5(5)
Bi(2)–O(2)	2.270(13)	O(2)–Bi(2)–O(6)	83.2(4)	O(6)–Bi(2)–O(10)^{i}	114.6(5)	O(7)^{i}–Bi(2)–O(10)^{i}	85.1(4)
Bi(2)–O(7)^{v}	2.356(14)	O(2)–Bi(2)–O(7)^{v}	88.5(5)	O(6)–Bi(2)–O(6)^{i}	116.3(3)	O(7)^{v}–Bi(2)–O(10)^{i}	79.1(6)
Bi(2)–O(6)	2.400(12)	O(2)–Bi(2)–O(10)^{i}	114.8(5)	O(6)–Bi(2)–O(7)^{v}	166.1(6)	O(7)^{v}–Bi(2)–O(7)^{i}	122.1(4)
Bi(2)–O(6)^{vi}	2.571(13)	O(2)–Bi(2)–O(7)^{i}	147.1(4)	O(6)^{i}–Bi(2)–O(7)^{i}	54.2(4)	O(9)–Bi(2)–O(7)^{v}	83.0(6)
Bi(2)–O1(0)^{vi}	2.702(13)	O(2)–Bi(2)–O(6)^{i}	151.7(5)	O(6)^{i}–Bi(2)–O(7)^{v}	68.0(5)	O(9)–Bi(2)–O(7)^{i}	93.0(6)
Bi(2)–O(7)^{vi}	2.756(16)	O(6)–Bi(2)–O(7)^{i}	64.3(4)	O(6)^{i}–Bi(2)–O(10)^{i}	77.1(4)	O(9)–Bi(2)–O(10)^{i}	157.4(5)
Bi(2)–O(1)	2.795(20)						
Bi(3)–O(1)	2.185(12) × 2	O(1)–Bi(3)–O(10)^{i}	74.8(5)	O(1)–Bi(3)–O(10)^{iv}	87.0(5)	O(8)^{iii}–Bi(3)–O(10)^{i}	112.0(4)
Bi(3)–O(10)^{vi}	2.404(13) × 2	O(1)–Bi(3)–O(8)^{v}	78.3(6)	O(1)–Bi(3)–O(8)^{iii}	159.7(5)	O(8)^{iii}–Bi(3)–O(8)^{v}	121.2(8)
Bi(3)–O(8)^{v}	2.604(13) × 2	O(1)–Bi(3)–O(1)^{ii}	83.2(8)	O(8)^{iii}–Bi(3)–O(10)^{iv}	80.3(4)	O(10)^{i}–Bi(3)–O(10)^{iv}	155.6(7)
Bi(3)–O(12)^{vi}	2.852(14) × 2						
PO_4 tetrahedra							
P(1)–O(4)	1.521(15)	O(1)–P(1)–O(2)	103.1(8)	O(1)–P(1)–O(4)	111.7(8)	O(2)–P(1)–O(3)	113.6(8)
P(1)–O(2)	1.554(15)	O(1)–P(1)–O(3)	103.6(8)	O(2)–P(1)–O(4)	113.3(9)	O(3)–P(1)–O(4)	110.9(9)
P(1)–O(3)	1.561(14)						
P(1)–O(1)	1.582(14)						
P(2)–O(5)	1.516(17)	O(5)–P(2)–O(8)	104.8(8)	O(5)–P(2)–O(7)	113.0(10)	O(6)–P(2)–O(6)	110.6(9)
P(2)–O(7)	1.523(16)	O(5)–P(2)–O(6)	111.2(8)	O(6)–P(2)–O(7)	104.6(8)	O(7)–P(2)–O(8)	112.8(9)
P(2)–O(8)	1.538(13)						
P(2)–O(6)	1.548(12)						
P(3)–O(11)	1.513(14)	O(9)–P(3)–O(12)	106.2(9)	O(9)–P(3)–O(10)	110.5(8)	O(10)–P(3)–O(10)	112.8(9)
P(3)–O(10)	1.547(12)	O(9)–P(3)–O(11)	106.1(8)	O(10)–P(3)–O(12)	105.4(7)	O(11)–P(3)–O(12)	115.7(7)
P(3)–O(12)	1.549(14)						
P(3)–O(9)	1.563(14)						
KO_8 polyhedra							
K(1)–O(4)^{iii}	2.635(15)	O(3)^{viii}–K(1)–O(4)^{viii}	50.9(4)	O(3)^{xi}–K(1)–O(7)^{v}	137.5(4)	O(7)^{v}–K(1)–O(9)	67.2(5)
K(1)–O(9)	2.703(15)	O(3)^{viii}–K(1)–O(5)^{v}	51.6(4)	O(3)^{xi}–K(1)–O(5)^{v}	147.9(4)	O(7)^{v}–K(1)–O(11)^{v}	94.1(4)
K(1)–O(7)^{v}	2.737(19)	O(3)^{viii}–K(1)–O(11)^{v}	56.9(3)	O(4)^{viii}–K(1)–O(1)1^{vii}	69.2(4)	O(7)^{v}–K(1)–O(12)	108.7(4)
K(1)–O(11)^{ii}	2.791(14)	O(3)^{viii}–K(1)–O(11)^{vii}	86.2(4)	O(4)^{viii}–K(1)–O(9)	76.0(5)	O(7)^{v}–K(1)–O(11)^{vii}	152.3(4)
K(1)–O(11)^{v}	2.861(16)	O(3)^{viii}–K(1)–O(7)^{v}	97.7(4)	O(4)^{viii}–K(1)–O7^{v}	92.0(5)	O(9)–K(1)–O(12)	50.6(4)
K(1)–O(3)^{xi}	3.051(16)	O(3)^{viii}-K(1)-O(3)^{xi}	117.7(3)	O(4)^{viii}–K(1)–O(5)^{v}	72.5(4)	O(9)–K(1)–O(11)^{vii}	88.0(4)
K(1)–O(12)	3.065(15)	O(3)^{viii}–K(1)–O(9)	124.9(4)	O(4)^{viii}–K(1)–O(12)	102.1(4)	O(9)–K(1)–O(11)^{v}	161.2(4)
K(1)–O(3)^{iii}	3.164(14)	O(3)^{viii}–K(1)–O(12)	143.4(3)	O(4)^{viii}–K(1)–O(11)^{v}	107.8(4)	O(11)^{v}–K(1)–O(12)	141.5(4)
		O(3)^{xi}–K(1)–O(12)	55.0(4)	O(5)^{v}–K(1)–O(7)^{v}	47.5(4)	O(11)^{vii}–K(1)–O(12)	58.7(4)
		O(3)^{xi}–K(1)–O(11)^{vii}	59.0(3)	O(5)^{v}–K(1)–O(11)^{v}	61.4(4)	O(11)^{vii}–K(1)–O(11)^{v}	110.7(4)
		O(3)^{xi}–K(1)–O(11)^{v}	87.2(4)	O(5)^{v}–K(1)–O(9)	103.9(4)		
		O(3)^{xi}–K(1)–O(9)	105.2(4)	O(5)^{v}–K(1)–O(1)1^{vii}	135.5(4)		
		O(3)^{xi}–K(1)–O(4)^{viii}	127.9(4)	O(5)^{v}–K(1)–O(12)	153.9(4)		
K(2)–O(8)	2.93(2) × 2	O(1)–K(2)–O(3)	51.0(4)	O(1)–K(2)–O(8)^{ii}	162.0(6)	O(8)–K(2)–O(12)^{xiii}	53.5(4)
K(2)–O(1)	2.61(2) × 2	O(1)–K(2)–O(1)^{ii}	67.6(7)	O(3)–K(2)–O(12)^{xiii}	54.5(4)	O(8)–K(2)–O(12)^{x}	81.6(5)
K(2)–O(3)	3.053(14) × 2	O(1)–K(2)–O(8)	95.8(4)	O(3)–K(2)–O(8)	61.8(4)	O(8)–K(2)–O(8)^{ii}	101.4(8)
K(2)–O(12)^{vii}	3.119(17) × 2	O(1)–K(2)–O(12)^{xiii}	105.0(4)	O(3)–K(2)–O(8)^{ii}	135.1(5)	O(8)–K(2)–O(3)^{ii}	135.1(5)
		O(1)–K(2)–O(3)^{ii}	108.6(6)	O(3)–K(2)–O(12)^{x}	143.0(5)	O(12)^{x}–K(2)–O(12)^{xiii}	108.4(8)
		O(1)–K(2)–O(12)^{x}	135.5(5)	O(3)–K(2)–O(3)^{ii}	158.5(8)		
K(1)–K(1)^{xii}	3.216(7)						

Symmetry transformations used to generate equivalent atoms: (i) $0.5-x$, $0.5-y$, $1-z$; (ii) $-x$, $-y$, $1-z$; (iii) $0.5-x$, $-0.5-y$, $1-z$; (iv) x, $1+y$, z; (v) x, $-1+y$, z; (vi) $0.5-x$, $-0.5+y$, $1.5-z$; (vii) $0.5-x$, $0.5+y$, $1.5-z$; (viii) $1-x$, y, $1.5-z$; (ix) $0.5+x$, $-0.5+y$, z; (x) $1-x$, $-1+y$, $1.5-z$; (xi) $-0.5+x$, $-0.5+y$, z; (xii) $-x$, $-1-y$, $1-z$; (xiii) $0.5+x$, $0.5+y$, z; (xiv) $-0.5+x$, $0.5+y$, z.

two parts with a particularly unchanged K_2MoO_4/MoO_3 ratio in the range of 0.23–0.06 and with $KPO_3/K_2MoO_4 =$ 16.16–5.21.

It is interesting to compare the results of the phase crystallization obtained for experimental points, which are quite close to the KPO_3–$K_2Mo_2O_7$ join. On the

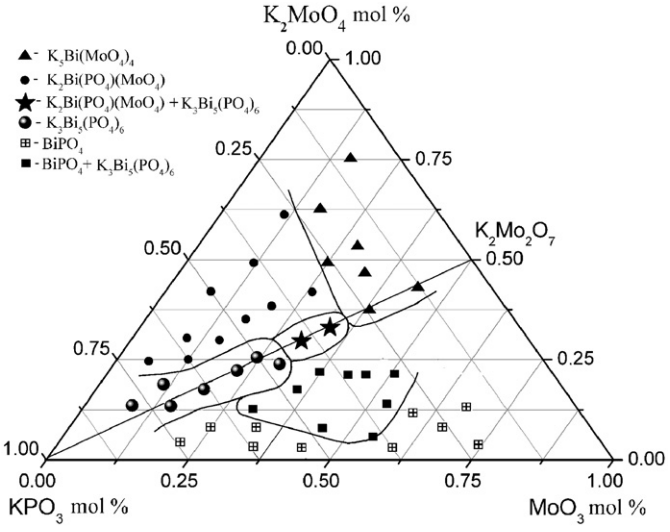

Fig. 1. Composition diagram of the K_2MoO_4–KPO_3–MoO_3 system containing 15 mol% Bi_2O_3 with approximate fields of phase formation. Each point on the ternary diagram xK_2MoO_4–$yKPO_3$–$zMoO_3$ corresponds to starting compositions of the quaternary system $0.85xK_2MoO_4$–$0.85yKPO_3$–$0.85zMoO_3$–$0.15Bi_2O_3$.

phosphate-rich side of this join, $K_3Bi_5(PO_4)_6$ crystallizes in case of molar ratios of $K_2Mo_2O_7/KPO_3 = 0.12$–0.54. Higher molar ratios (0.78–1.00) cause the appearance of $K_2Bi(PO_4)(MoO_4)$ as an additional phase (3–23% yield). Finally, increase of molar ratio of $K_2Mo_2O_7/KPO_3$ up to 3.75 leads to $K_5Bi(MoO_4)_4$ crystallization. In this context, decrease of K_2MoO_4 content for the investigated system causes the crystallization of HT-$BiPO_4$, whereas the formation of more potassium-rich compounds is observed for melts rich in potassium.

Logically, the composition of melts is changing significantly during crystallization process due to formation of solid phase. Comparison of these changes before and after crystallization of bismuth-containing compounds can be illustrated by the following formal schemes:

$$5K_2Mo_2O_7 + Bi_2O_3 \rightarrow 2K_5Bi(MoO_4)_4 + 2MoO_3, \quad (1)$$

$$2KPO_3 + K_2Mo_2O_7 + Bi_2O_3 \rightarrow 2K_2Bi(PO_4)(MoO_4), \quad (2)$$

$$12KPO_3 + 5Bi_2O_3 \rightarrow 2K_3Bi_5(PO_4)_6 + 3K_2O^*, \quad (3)$$

$$2KPO_3 + Bi_2O_3 \rightarrow 2BiPO_4 + K_2O^*, \quad (4)$$

where * represents absorbed by molybdate melt.

From this point of view, phase formation indicated at the composition diagram (Fig. 1) can be specified on three parts. Appearance of $K_5Bi(MoO_4)_4$ makes melt richer in MoO_3 (Eq. (1)). The same equation illustrates the conventional flux method used for preparation of this molybdate from $K_2Mo_2O_7$ flux [27]. In this case the low content of KPO_3 could be presented as an inert background. During $K_2Bi(PO_4)(MoO_4)$ crystallization, the solution becomes poorer on both phosphate and molybdate parts (Eq. (2)) and the corresponding melt can be considered as the usual self-flux.

Biphasic and pure phosphate fields should be discussed separately. Thus, after formation of $K_3Bi_5(PO_4)_6$ the remaining melt is enriched by the molybdate part, which absorbs redundant K_2O as is shown in Eq. (3). Increasing the molybdenum content accompanied by rising of absorbed K_2O (Eq. (4)) leads to cocrystallization of $K_3Bi_5(PO_4)_6 + BiPO_4$ and finally to pure $BiPO_4$. As a result, molybdate can be seen as a soft regulator of crystallization pathways with respect to the phosphate part, which sets the type of appearing solid phase. Possibility of smooth regulation may be proved on the evidence of broad biphasic regions and the existence of $K_3Bi_5(PO_4)_6$. Strangely, the latter phosphate had not been obtained using pure phosphate melts KPO_3–Bi_2O_3 [28].

Consequently, variation of the $MoO_3/K_2MoO_4/KPO_3$ ratios to cause crystallization of the desired phases may be successfully applied to other phosphate-containing systems.

3.2. Crystal structure $K_3Bi_5(PO_4)_6$

The structure consists of packed BiO_8 polyhedra and PO_4 tetrahedra, delimiting channels where potassium cations are located. Three unique bismuth atoms are eight-coordinated with Bi–O distances ranging from 2.183(15) to 2.852(14) Å (Fig. 2). Both Bi(1) and Bi(2) atoms occupy general positions and possess significantly irregular oxygen environments. The third Bi(3) atom resides in a special position owning regular dodecahedral polyhedron with four pairs of equidistant Bi–O length distances. The phosphorus atoms are located in *8f* sites that are surrounded by four oxygen atoms in a tetrahedral arrangement. The orthophosphate tetrahedra geometry is close to regular with the P–O bond length ranging from 1.513(14) to 1.582(14) Å, and the O–P–O angles spread over the range 103.(8)–115.7(7)°.

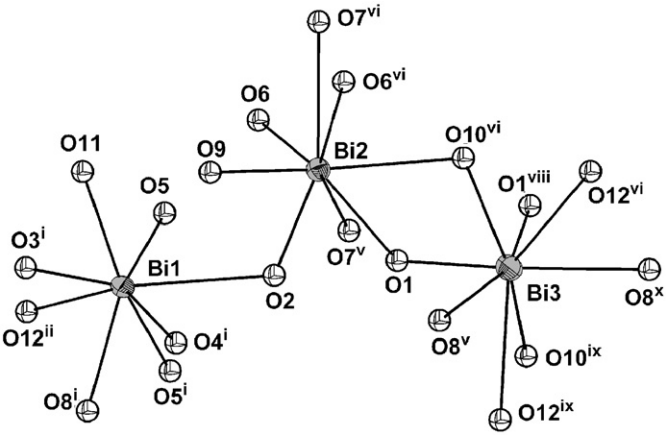

Fig. 2. The oxygen coordination of the bismuth atoms in $K_3Bi_5(PO_4)_6$ (symmetry code: (i) $0.5-x$, $-0.5+y$, $1.5-z$; (ii) $1-x$, y, $1.5-z$; (v) x, $-1+y$, z; (vi) $0.5-x$, $0.5-y$, $1-z$; (viii) $0.5-x$, $-0.5-y$, $1-z$; (ix) x, $1+y$, z; (x) $0.5-x$, $0.5+y$, $1.5-z$).

Anionic fragment $[Bi_5P_6O_{40}]$ could be selected as a building block of this structure. It contains $Bi(3)O_8$ dodecahedron, which shares its edges with two pairs of Bi(1) and Bi(2) polyhedra including six PO_4 groups (Fig. 3). The linkage between those blocks is achieved by sharing vertices of bismuth polyhedra and additionally fixed by corner-sharing phosphate groups.

One remarkable feature of this structure concerns the geometry of six BiO_8 connected by their edges and vertices into a ring (Fig. 4a). This is an unusual assemblage of bismuth polyhedra in oxide compounds and was observed for the first time in $LiRbBi_2(MoO_4)_4$ [29]. This connection between two neighboring rings through the common $Bi(3)O_8$ gives rise to the formation of a zig-zag chain in the crystallographic direction [101] (Fig. 4b). Both $Bi(1)O_8$ and $Bi(2)O_8$ polyhedra share two common edges with $Bi(1)O_8$ and $Bi(2)O_8$ from the adjacent chain $(BiO_8)_6$ forming a 3D framework. It is noteworthy that this linkage leads to formation of the eight-member rings with semicircle $[Bi(1)O_8–Bi(2)O_8–Bi(2)O_8–Bi(3)O_8]_2$. The general architecture of the formed $(BiO_8)_6$, $(BiO_8)_8$ and $(BiO_8)_{12}$ circles is given in Fig. 4c.

Principles of the linkage of BiO_8 and PO_4 groups are shown in Fig. 5. They are similar for $P(1)O_4$ and $P(3)O_4$ tetrahedra. Formation of four-member planar rings BiO_2P with a bidentate type of coordination is observed for two adjacent bismuth atoms. Additional connection with other two bismuth atoms is made via opposite oxygen atoms. Linkages of $P(2)O_4$ and BiO_8 polyhedra differ remarkably from other phosphate groups in this structure but it is very similar to those observed in $BiPO_4$ [25] and $K_2Bi(PO_4)(MoO_4)$ [22].

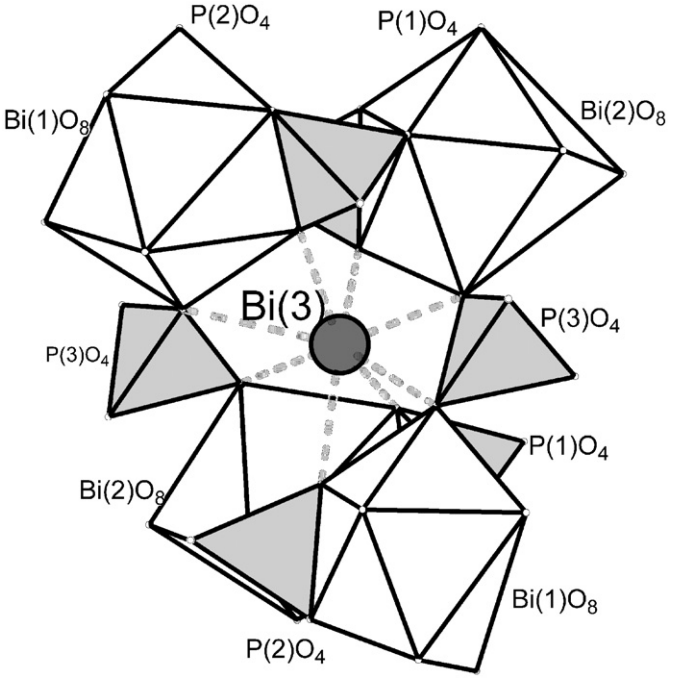

Fig. 3. View of $[Bi_5P_6O_{40}]$ building unit.

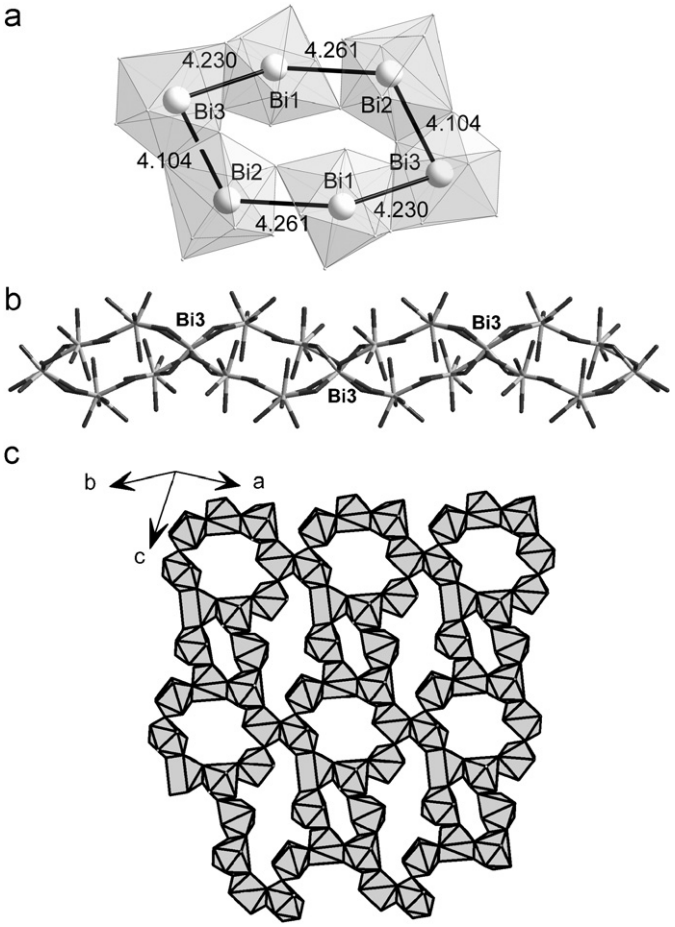

Fig. 4. The principles of bismuth polyhedra connections in $K_3Bi_5(PO_4)_6$: (a) six-member ring built from BiO_8 polyhedra; (b) zig-zag $[(BiO_8)_6]_\infty$ chain formation along the [101] direction; and (c) three types of $(BiO_8)_6$, $(BiO_8)_8$ and $(BiO_8)_{12}$ rings in a 2D network.

Sublattice $[Bi_5(PO_4)_6]$ is penetrated by a system of zig-zag channels along direction *c* where potassium atoms are located (K(1) in *8f* and K(2) in 4*e* positions). A pair of K(1) atoms exist inside the "crown" of an eight-member $(BiO_8)_8$ ring with eight phosphate tetrahedra (Fig. 6a). The nearest distance of K(1)–K(1) is equal to 3.216(7) Å. All potassium atoms have eight-fold oxygen coordinations with cut-off distance 3.2 Å. The cavity where the K(2) atom resides is formed by six BiO_8 polyhedra and six PO_4 groups (Fig. 6b). The nearest distance between K(1) and K(2) is 4.184(3) Å.

3.3. FTIR spectra

IR spectra (Fig. 7) for obtained phosphates $BiPO_4$ (HT) and $K_3Bi_5(PO_4)_6$ show several bands in the 1150–850 cm^{-1} region belonging to the characteristic ν_1, ν_3 (P–O) vibrations of the PO_4 group as well as multiple bands in the 650–500 cm^{-1} region for ν_2 and ν_4 (PO_2) modes [30]. The observed shape of the $BiPO_4$ (HT) spectrum absolutely correlates with earlier reported data [31]. For the $K_3Bi_5(PO_4)_6$ spectrum in diapason 1150–850 cm^{-1} six phosphate vibration lines can be easily selected (Fig. 7).

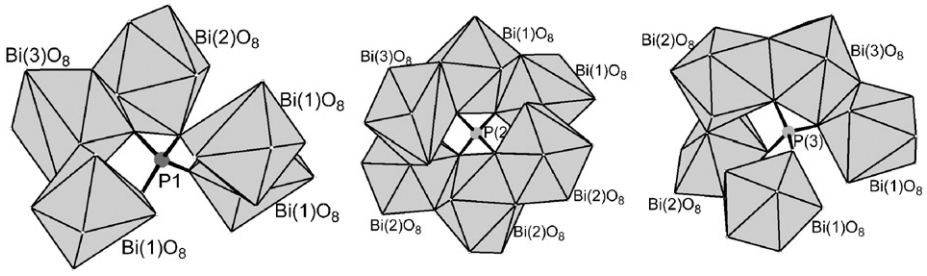

Fig. 5. Arrangement of phosphorus tetrahedra by bismuth polyhedra.

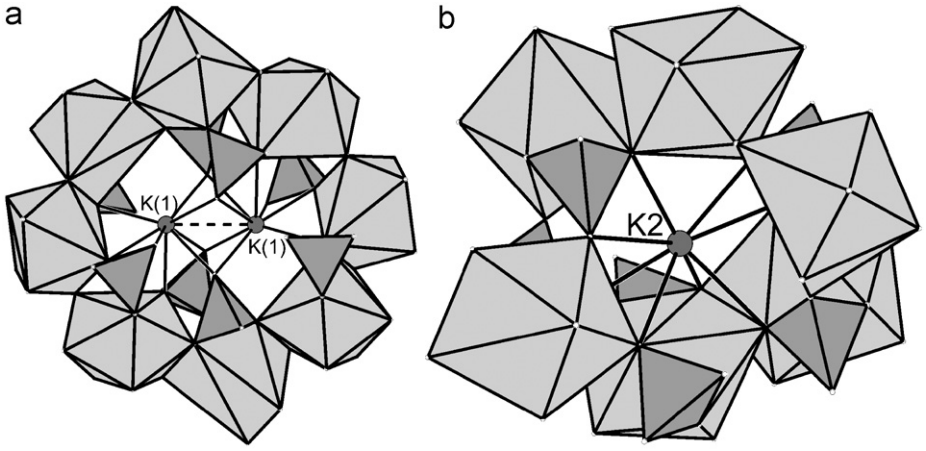

Fig. 6. Potassium atoms localization in the $K_3Bi_5(PO_4)_6$ structure: (a) a pair of K(1) atoms exist inside the "crown" of eight-member $(BiO_8)_8$ and (b) the cavity where K(2) atom resides.

Their wider expansion compared with those observed for $BiPO_4$ is more likely connected with the existence of three types of PO_4 groups with low local symmetry (Table 3).

The IR spectrum of $K_2Bi(PO_4)(MoO_4)$ had been discussed earlier in [22].

3.4. Characterization of the Voronoi–Dirichlet bismuth polyhedra and lone electron pair stereoactivity

Two prepared compounds $K_3Bi_5(PO_4)_6$ and $K_2Bi(PO_4)(MoO_4)$ were investigated with respect to the lone electron pair stereoactivity of bismuth. Calculations of all the characteristics of the Voronoi–Dirichlet polyhedra (VDP) were performed with the TOPOS program package [32].

The volumes of the VDP of the Bi(1), Bi(2) and Bi(3) atoms in the $K_3Bi_5(PO_4)_6$ structure are 12.6, 13.4 and 13.0 $Å^3$, respectively, which agree well with the average value (13.2(7) $Å^3$) found for Bi(III) atoms (CN = 8) surrounded by oxygen atoms [33]. The VDP of all Bi atoms are strongly distorted. An example is provided by the VDP of the Bi(1) (Fig. 8). It should be emphasized that all Bi atoms in the structure of $K_3Bi_5(PO_4)_6$ are substantially displaced from the VDP centers of gravity. The values of displacement (D_A) [34] are 0.15, 0.20 and 0.18 Å for Bi(1)–Bi(3), respectively, which is due to the fact that the electron density distribution around the Bi(III) atoms is anisotropic because of the presence of an active lone electron pair.

The values of displacement $D_A = 0.001 \approx 0$ Å for the Bi atom in the structure of $K_2Bi(PO_4)(MoO_4)$ indicating that the lone electron pair is inactive.

4. Conclusion

In the presented work the composition diagram for the K_2MoO_4–KPO_3–MoO_3 system containing 15 mol% Bi_2O_3 is reported and briefly discussed. Fields of three known and one new $K_3Bi_5(PO_4)_6$ compounds were constructed as a result of slow cooling and spontaneous crystallization. The structure of $K_3Bi_5(PO_4)_6$ forms a 3D framework, which is built up from BiO_8 corner-sharing polyhedra and PO_4 groups with delimiting channels where potassium cations are located. The possibility of lone electron pair activity of bismuth was suggested using the calculations of characteristics of the VDP for $K_3Bi_5(PO_4)_6$ and $K_2Bi(PO_4)(MoO_4)$.

The role of soft regulator of crystallization pathways was illustrated for the molybdate part of phosphate-molybdate melts with respect to the phosphate part. This approach could be applied to other complex phosphate-containing systems.

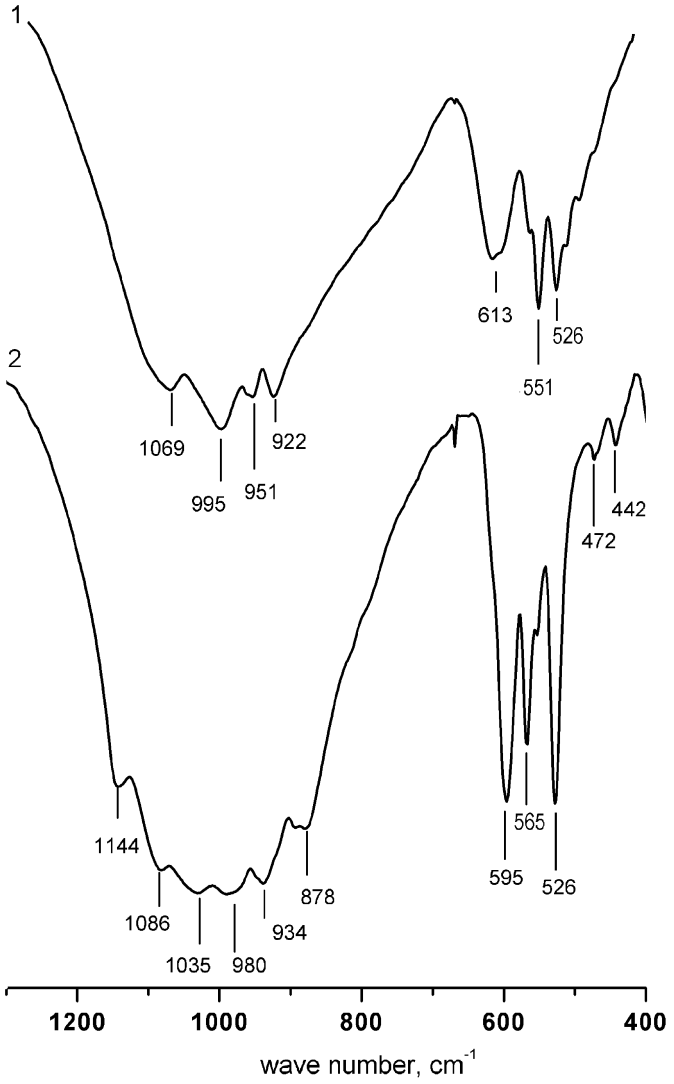

Fig. 7. FTIR spectra of $BiPO_4$(HT) (1) and $K_3Bi_5(PO_4)_6$ (2).

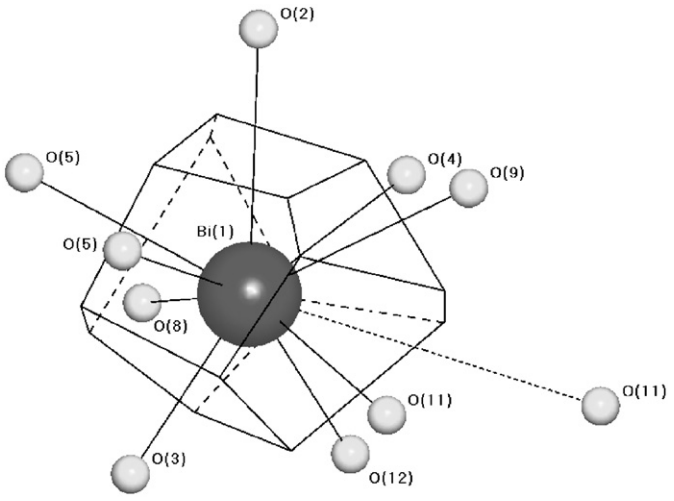

Fig. 8. The Voronoi–Dirichlet polyhedron of the Bi(1) in the $K_3Bi_5(PO_4)_6$ structure.

Acknowledgment

The authors acknowledge the ICDD for financial support (Grant #03-02).

References

[1] E. Arbib, B. Elouadi, J.P. Chminade, J. Darriet, Mater. Res. Bull. 35 (2000) 761–773.
[2] E. Arbib, J.P. Chminade, J. Darriet, B. Elouadi, Solid State Sci. 2 (2000) 243–247.
[3] J. Darriet, J.C. Launay, F.J. Zugina, J. Solid State Chem. 178 (2005) 2015–2023.
[4] B. Delmon, M. Ruwet, S. Ceckiewicz, Ind. Eng. Chem. Res. 26 (1987) 1981–1986.
[5] J.C. Jung, H. Kim, A.S. Choi, Y.-M. Chung, T.J. Kim, S.J. Lee, S.-H. Oh, I.K. Song, J. Mol. Catal. A: Chem. 259 (2006) 166–170.
[6] J.C. Jung, H. Kim, Y.-M. Chung, T.J. Kim, S.J. Lee, S.-H. Oh, Y.S. Kim, I.K. Song, J. Mol. Catal. A: Chem. 264 (2007) 237–240.
[7] J.C. Jung, H. Kim, A.S. Choi, Y.-M. Chung, T.J. Kim, S.J. Lee, S.-H. Oh, I.K. Song, Catal. Commun. 8 (2007) 625–628.
[8] C. Cascales, A. Méndez Blas, M. Rico, V. Volkov, C. Zaldo, Opt. Mater. 27 (2005) 1672–1680.
[9] H. Cañibano, G. Boulon, L. Palatella, Y. Guyot, A. Brenier, M. Voda, R. Balda, J. Fernández, J. Lumin. 102–103 (2003) 318–326.
[10] M. Rico, V. Volkov, C. Cascales, C. Zaldo, Chem. Phys. 279 (2002) 73–86.
[11] S.S. Gerashchenko, O.V. Miloslavskaya, Yu.N. Kharchenko, V.I. Kut'ko, N.M. Nesterenko, L. Macalik, K. Hermanowicz, J. Hanuza, J. Mol. Struct. 563–564 (2001) 359–364.
[12] S. Giraund, M. Drache, P. Conflant, J.P. Wignacourt, H. Steinfink, J. Solid State Chem. 154 (2000) 435–443.
[13] M.F. Debreuille-Gresse, M. Drache, F. Abraham, J. Solid State Chem. 62 (1986) 351–359.
[14] M. Diouri, A. Sadel, M. Zahir, M. Drache, P. Conflant, J.P. Wignacourt, J.C. Boivin, J. Alloys Compd. 188 (1992) 206–210.
[15] M. Ketatni, O. Mentre, F. Abraham, B. Mernari, J. Solid State Chem. 139 (1998) 254–280.
[16] M. Watanabe, T. Yamada, Mem. Coll. Eng. Chubu Univ. 21 (1985) 53–61.
[17] A. Chahine, M. Et-Tabirou, J.L. Pascal, Mater. Lett. 58 (2004) 2776–2780.
[18] A.A. Babaryk, I.V. Zatovsky, V.N. Baumer, N.S. Slobodyanik, P.G. Nagorny, O.V. Shishkin, J. Solid State Chem. 180 (2007) 1990–1997.
[19] I. Koseva, V. Nikolov, P. Peshev, J. Alloys Compd. 353 (2003) L1–L4.
[20] B. Lajmi, M. Hidouri, A. Wattiaux, L. Fournes, J. Darriet, M. Ben Amara, J. Alloys Compd. 361 (2003) 77–83.
[21] M. Hidouri, B. Lajmi, A. Wattiaux, L. Fournes, J. Darriet, M. Ben Amara, J. Alloys Compd. 358 (2003) 36–41.
[22] I.V. Zatovsky, K.V. Terebilenko, N.S. Slobodyanik, V.N. Baumer, O.V. Shishkin, J. Solid State Chem. 179 (2006) 3550–3555.
[23] G.M. Sheldrick, SHELXS-97, University of Göttingen, Germany, 1997.
[24] G.M. Sheldrick, SHELXL-97: Program for Crystal Structure Refinement, University of Göttingen, Germany, 1997.
[25] R. Masse, A. Durif, C. R. Acad. Sci. 300 (1985) 849–851.
[26] V.A. Efremov, B.M. Lazoryak, Kristallografiya 31 (1986) 237–243.
[27] P.V. Klevtsov, V.A. Vinokurov, Izv. Akad. Nauk SSSR Neorg. Mater. 11 (1975) 387–388 (in Russian).
[28] S.I. Berul, S.V. Solodzy, Russ. J. Inorg. Chem. XIV (1969) 3134–3139 (in Russian).
[29] R.F. Klevtsova, L.A. Glinskaya, V.I. Alekseev, K.M. Khalbaeva, E.G. Khaikina, J. Struct. Chem. 34 (1994) 789–793.
[30] K. Nakamoto, Infrared and Raman Spectra of Inorganic and Coordination Compounds, fourth ed, Wiley, New York, 1986.

[31] N.N. Chudinova, L.A. Tezikova, B.B. Sedov, Izv. Akad. Nauk SSSR Neorg. Mater. 9 (1973) 2033–2036 (in Russian).
[32] V.A. Blatov, A.P. Shevchenko, V.N. Serezhkin, J. Appl. Crystallogr. 33 (2000) 1193–1196.
[33] D.V. Pushkin, E.A. Sokolova, V.N. Serezhkin, Russ. J. Coord. Chem. 26 (2000) 1–5.
[34] V.N. Serezhkin, Yu.A. Buslaev, Russ. J. Inorg. Chem. 42 (1997) 1064–1071.